Nature Environment and Pollution Technology
An International Quarterly Scientific Journal

p-ISSN: 0972-6268 e-ISSN: 2395-3454	Vol. 17	No. 2	pp. 469-478	2018

Original Research Paper | Open Access

Synthesis and Characterization of Chitosan Nanoparticles and Their Application in Removal of Wastewater Contaminants

Pritha Chakraborty, Vakas Mustafa and Jayanthi Abraham†
Microbial Biotechnology Lab, School of Biosciences and Technology, VIT University, Vellore-632 014, T. N., India
†Corresponding author: Jayanthi Abraham

Nat. Env. & Poll. Tech.
Website: www.neptjournal.com

Received: 15-08-2017
Accepted: 25-09-2017

Key Words:
Chitosan nanoparticles
Ionic gelation
Adsorption kinetics
Wastewater contaminants
Degradation

ABSTRACT

The purpose of this study was to synthesise, characterize and evaluate environmental application (degradation of dyes and pesticides) of chitosan nanoparticles. The chitosan nanoparticles were synthesized by ionic gelation process and characterized. The physicochemical properties of the nanoparticles were determined by size and zeta potential analysis, scanning electron microscope (SEM), atomic force microscopy (AFM), FTIR analysis and XRD pattern. The photocatalytic degradation was studied with the help of industrial dyes, and pesticides. Adsorption experiments were carried out to highlight the adsorption efficiency of the organic compound with different parameters like pH, dosage and time. A sharp increase in the percent reduction of dyes and pesticides was observed as the adsorbent dose increased. The kinetic data were modelled with the pseudo first-order and pseudo second-order kinetic equations.

INTRODUCTION

Chitosan is a polysaccharide, similar in structure to cellulose. Both are made by linear h-(1Y4)-linked monosaccharides. However, an important difference to cellulose is that chitosan is composed of 2-amino-2-deoxy-h-d-glucan combined with glycosidic linkages. The primary amine groups render special properties that make chitosan very useful in pharmaceutical applications. Compared to many other natural polymers, chitosan has a positive charge and is mucoadhesive (Berscht et al. 1994). Therefore, it is used extensively in drug delivery applications.

Chitosan is a cationic biopolymer obtained from deacetylation of chitin which is the second most abundant biopolymer in nature. Chitosan nanoparticles have been synthesized as drug carriers as reported in previous studies. Insulin loaded chitosan nanoparticles could enhance intestinal absorption of insulin and increase its relative pharmacological bioavailability. Chitosan nanoparticles had also been employed as a gene carrier to enhance gene transfer efficiency in cells (Ngah et al. 2011).

Various Studies have shown that chitosan nanoparticles can carry many drugs including gene drugs, protein drugs, anticancer chemical drugs, and antibiotics, and via various routes of administration like oral, nasal, intravenous, and ocular. Chitosan nanoparticles can be used as a gene carrier. As a nonviral carrier, chitosan has excellent biocompatibility and biodegradation, which has led to increasing application of chitosan nanoparticles in gene drug delivery (Katas et al. 2013). Protein drugs can be degraded easily by enzymes *in vivo* and have poor permeability and stability as well as a short half-life. However, chitosan can protect protein well and promote the contact between drug and bio-membrane, thereby improving bioavailability (Amidi et al. 2011).

Chitosan has been used as an excellent natural adsorbent to remove many pollutants including dyes, heavy metals and fluoride due to the presence of amino and hydroxyl groups (Miretzky & Cirelli 2011). However, information regarding chitosan nanoparticles in environmental application is found to be inadequate, hence this aspect of chitosan nanoparticles in degradation of dyes and pesticides was explored in this study.

MATERIALS AND METHODS

Chemicals: Chitosan with degree of acetylation 85% and molecular weight 2.6×10^5 was purchased from Sigma Aldrich. Sodium tripolyphosphate (STTP), acetic acid (CH_3COOH), methylene blue (MB) and orange dyes were of analytical grade and also purchased from Sigma Aldrich. Deionized water was used throughout the studies.

Preparation and characterization of chitosan nanoparticles: Chitosan nanoparticles were prepared by ionic gelation process. Chitosan was dissolved in 0.5% acetic acid solution at a concentration of 3 mg/mL. A solution of TPP at the concentration of 1.0 mg/mL was prepared with

deionized water. Then, 10 mL of TPP solution was added drop wise to 25 mL of the chitosan solution under constant stirring condition. An opalescent suspension was formed spontaneously under these conditions. Nanoparticles were separated by centrifugation at 16,000 rpm for period of 30 min at 14°C. The supernatant was discarded and the wet pellet of chitosan nanoparticles was collected. The pellet was washed with 20, 75 and 100% ethanol followed by freeze drying, and stored at 4°C for further studies (Vimal et al. 2012).

Particle size distribution and zeta potential: Mean particle size (Z-average) and zeta potential of the nanoparticles were measured by using Malvern ZetasizerNano ZS (UK). The measurements were performed at a temperature of 25°C in triplicate. Samples were appropriately diluted with methanol prior to measurement. The values were reported as mean ± standard deviation (Jiang et al. 2009).

Scanning electron microscope (SEM): The morphology of the chitosan nanoparticles was observed by field emission scanning electron microscopy (FE-SEM) (AMRAY1910) equipped with a backscattered electron detector at 15-30 kV. For SEM images, the samples were sputter-coated with about 15 nm Au using a Polaron coater system (Jayakumar et al. 2009).

FT-IR: The Fourier Transform Infrared Spectra (FTIR) of chitosan nanoparticles was recorded on a Perkin-Elmer FTIR spectrometer (SPECTRUM 1000) using KBr pellets at a resolution of 4 cm^{-1} to evaluate the cross-linking of chitosan with TPP. The chitosan nanoparticles were mixed with KBr in the ratio of 1:150 and ground in a mortar by hand with a pestle. The powder was pressed into pellets under a pressure of 4t. The IR absorbance scans were analysed from 400 to 4000 cm^{-1} in the intensity of the sample peaks (Dounighi et al. 2012).

Atomic Force Microscope (AFM): Atomic force microscopy (AFM, SPM-9500J3) was used for visualization of chitosan nanoparticles deposited on silicon substrates operating in the contact mode. The samples were analysed by contact mode with Si3N4 tip having a force constant of 0.12 N/m. The presence of elements and chemical states of the catalysts were examined by ESCALAB 200 X-ray photoelectron spectrophotometer (VG Scientific) with monochromatic Mg Kα excitation source. The pressure was maintained at 6.3×10-5 Pa. Prior to XPS measurements all as sprayed samples were calcinated at 400°C for 2 h to ensure that any possible residual precursors would decompose completely (Motwani et al. 2008).

X-Ray Diffraction (XRD): The phase and crystallinity were characterized by using a Rigaku D/max-2500 X-ray diffractometer with Cu Kα radiation in the 2h range of 10-80° (Lim et al. 2003).

UV-visible absorption: UV-visible absorption spectra of the samples were obtained using a Schimadzu, UV-2101 spectrophotometer, to study the optical absorption properties of the photocatalyst. The spectra were recorded at room temperature in the wavelength range 200-800 nm enabling to understand the spectral properties of chitosan nanoparticles (Janes et al. 2001).

Degradation of Pollutants

Dye degradation: 50 ppm of dye (Blue and orange) solution was prepared separately using distilled water and made up to 50mL. 100mg/L, 200mg/L and 300mg/L concentration of chitosan nanoparticles was added in the dye solution. The dye and nanoparticle mixture was continuously stirred on magnetic stirrer for 30 min. The sample mixture was kept under UV light for photocatalytic degradation. After 30 min, 60 min and 90 min and continuously till 180 min time interval, 3 mL of the sample was withdrawn and centrifuged at 4000 rpm for 30min. The supernatant solution was used to check the absorbance at 365 nm with the help of a spectrometer. The dye degradation percentage with the help of nanoparticles was calculated by the formula:

$$\text{Percent of degradation} = [(C_0 - C_t)/C_0] \times 100$$

Where, C_0 = initial concentration of dye; C_t = dye concentration after time t.

Pesticide Degradation: Two predominantly used pesticides profenofos and lambda cyhalothrin were chosen for this study. 100 mg chitosan nanoparticles were added in 100 mL of individual pesticide (Profenofos and Lambda cyhalothrin) to aqueous solution (100mL distilled water + 100µL pesticide). The solution was kept under the UV light for 24 hours. After that the next 5 days UV irradiated 5 mL aliquots were withdrawn from the suspension at specific interval of time. The aliquots centrifuged at 1500 rpm for 30 min, and then it was filtered through Whatman filter paper to remove the suspended particles. The filtrate was analysed by HPLC method (Yongmei & Yumin 2003).

The HPLC analysis was performed on isocratic system using a Shimadzu chromatograph including LC-10 AS pumps, 20-11 reodyne injector, SPD-10A UV-detector operating at 208 nm and Supelco C18 Cartridge column (25cm-6mm). A mixture of acetonitrile (ACN) and water (80:20) mixture were used as mobile phase for removal of any impurity, bubbles and dissolved oxygen, double distilled water and acetonitrile was first passed through 0.45µm micropore filter paper with filtration assembly and then sonicated for 10 mins. The flow rate was kept at 1mL/min, injection volume was 10µL, and run time was 25 min.

Kinetic Studies

Kinetic studies for dye degradation: A stock solution was

prepared with the help of dye solution and water without the photo catalyst in the range of 5-50ppm. The absorbance was recorded at 620nm and calibration curve was plotted. The maximum absorbance showing the ppm was used as standard initial concentration. The 50 ppm dye (Blue) solution was prepared with the help of water and made up to 50 mL. Firstly, the pH was standardized with 5 different pH ranges of 2, 4, 6, 8 and 10 with roughly 50 mg of chitosan nanoparticles and it was kept in orbital shaker for 1 hour at 100 rpm, this was filtered and the absorbance was checked at 620nm. After this the nanoparticles dosage were standardized with 5 different concentrations ranging from 20-60 mg with the standardized particular pH and maintaining the same incubation and reading procedure. Lastly, after standardization of particular pH and dosage, the effect of time was checked with 10 different flasks of same volume with standardized pH and dosage flasks were incubated on orbital shaker and after every 10 min 3 mL of sample was taken and the absorbance was checked (Wang et al. 2007).

Kinetic studies for pesticide degradation: Initial concentration of the pesticide was determined with the help of stock solution containing pesticide and water in the range of 5-50 ppm. The absorbance was recorded and a calibration graph was plotted. The highest absorbance was used as initial concentration for rest of the study. 50 mL pesticide (lambda cyhalothrin) stock solution was prepared maintaining the concentration at 50 ppm. pH was optimized with five different pH ranges of 2, 4, 6, 8 and 10 with 30mg chitosan nanoparticles. After one hour incubation on shaker, 3 mL of the sample was withdrawn and filtered with Whatman filter paper and absorbance was checked at 340nm. The dosage was optimized with five different concentrations within the range of 10-50mg and the standardized pH from previous studies. The effect of time was checked with 10 different flasks of same volume with standardized pH and dosage flasks were incubated on orbital shaker and after every 10 min 3 mL of sample was taken and the absorbance was checked (Daneshvar et al. 2007).

RESULTS AND DISCUSSION

Characterization

Particle size distribution and zeta potential: The preparation of chitosan nanoparticles is based on an ionic gelation interaction between positively charged chitosan and negatively charged tripolyphosphate at room temperature (Knaul et al. 1999). The chitosan nanoparticles prepared in the experiment exhibit a white powdered appearance and are insoluble in water and dilute acids. The mean size and size distribution of each batch of nanoparticle suspension was analysed using the Zetasizer analysis. The size distribution profile, as shown in Fig. 1, represents a typical batch of nanoparticles with a mean diameter of 90.9 nm and a narrow size distribution (polydispersity index <1).

Zeta potential, that is, surface charge, can greatly influence the particle stability in suspension through electrostatic repulsion between particles. Zeta potential measurement is used to analyse the nanoparticle interaction with the cell membrane of bacteria (Patil et al. 2007), which is negatively charged. Fig. 2 shows the zeta potential measurement of chitosan nanoparticles. The chitosan nanoparticle has a negative surface charge of about -21.2mV.

Scanning Electron Microscopy (SEM): SEM analysis is another useful tool for the surface morphology of synthesized chitosan nanoparticles which is presented in Fig. 3. From the surface SEM micrographs it suggests that the crosslinked chitosan was gradually produced after cross linking with sodium tripolyphosphate in alkaline solution (Abraham et al. 2016). Result confirms the crosslinking of chitosan.

FT-IR: Chitosan nanoparticles were prepared with chitosan and tripolyphosphate. FTIR studies of chitosan nanoparticle were performed to characterize the chemical structure of nanoparticles. FTIR spectra of chitosan nanoparticles are shown in Fig. 4.

The peak located at 1741cm^{-1} indicates the carbonyl stretching of chitosan nanoparticles. The band shifts from 1635cm^{-1} and 1537cm^{-1}, correspond to C-O and N-H stretching. The peaks at 1369cm^{-1} correspond to the stretching of carboxylate has been detected. The peak at 1369 cm^{-1} can be attributed to the CH_3 symmetric deformation and the peak at 1215cm^{-1} corresponds to the C-O stretching. A new IR band at 1026cm^{-1} was assigned to N-H deformation, C_3-OH and C_6-OH stretching, respectively. Two sorption bands at 1635 cm^{-1} and 1537 cm^{-1} appear which show that the ammonium groups are cross linked with tripolyphosphate molecules. It shows that polyphosphoric groups of sodium polyphosphate interact with the ammonium groups of chitosan, which serves to enhance both inter and intramolecular interaction in chitosan nanoparticles. Similar results were also observed in a previous study by Lifeng et al. (2004).

AFM (Atomic Force Microscope): AFM image was taken with silicon cantilevers with constant force of 0.02-0.77N/m, tip height 10-15 nm, contact mode. Fig. 5 shows the image of irregular chitosan nanoparticles, it can be clearly seen as nanoisland formation apart from that there is prominent agglomeration of chitosan (Abraham et al. 2013). The size of chitosan nanoparticles ranged from 89.1-103nm.

XRD (X-Ray Diffraction): X-Ray powder diffraction patterns of chitosan nanoparticles are shown in Fig. 6. However, no peak is found in the diffractograms of chitosan

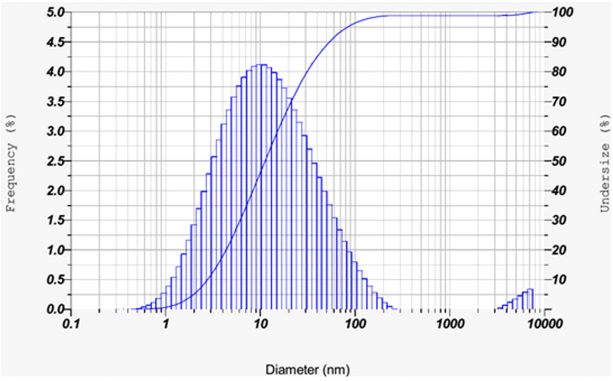

Fig. 1: The size distribution by frequency of chitosan nanoparticles.

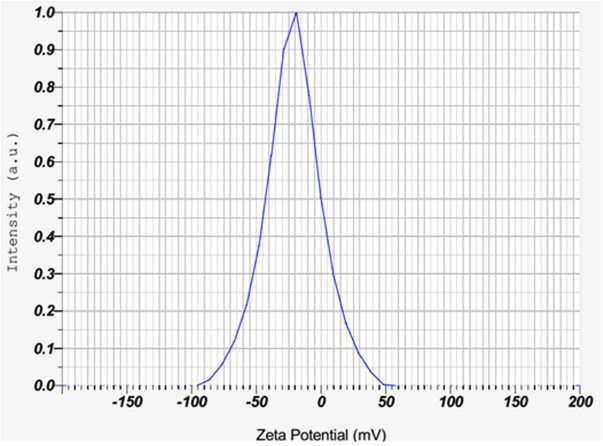

Fig. 2: Zeta potential distribution of chitosan nanoparticles.

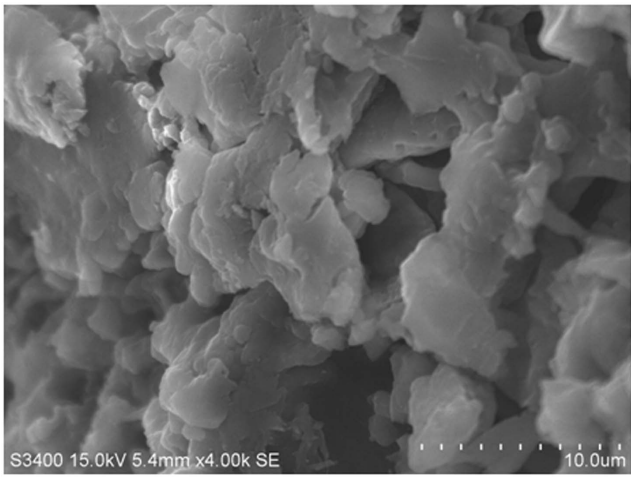

Fig. 3: SEM image of chitosan nanoparticles.

nanoparticles (Tang et al. 2003). Chitosan nanoparticles are comprised of a dense network structure of interpenetrating polymer chains cross linked to each other by TPP counter ions (Huang et al. 2004). The XRD implicated greater

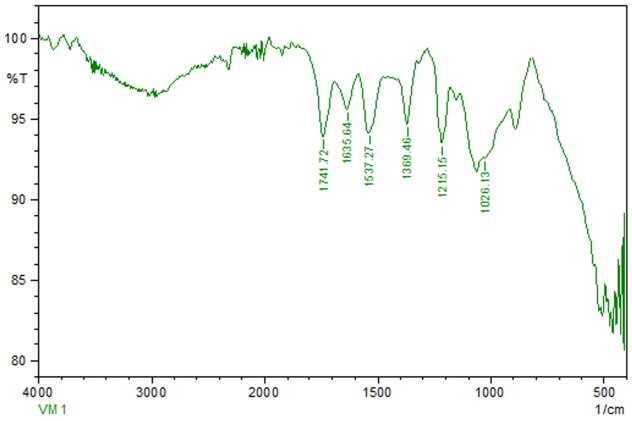

Fig. 4: FTIR spectra of chitosan nanoparticles.

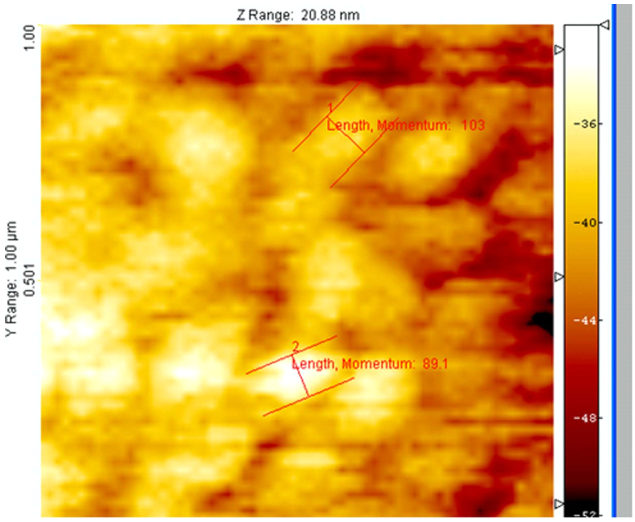

Fig. 5: AFM image of chitosan nanoparticles.

disarray in chain alignment in the nanoparticles after cross linking.

UV-Visible absorption: The UV-VIS absorption spectrum can be considered as a promising operation for chitosan nanoparticles processing. The characterization done using UV-VIS spectrophotometry analysed the formation and stability of the chitosan nanoparticles in the colloidal solution at different irradiation time intervals. Fig. 7 shows the spectra exhibiting an absorption band at around 400nm, which is a typical Plasmon band, suggesting the formation of chitosan nanoparticles. The centre of absorption band also varied slightly with chitosan molecular weight, a factor that operates as a controller of nucleation as well as stabilization (Park et al. 2012).

Degradation Studies

Dye degradation: The three different concentrations (100

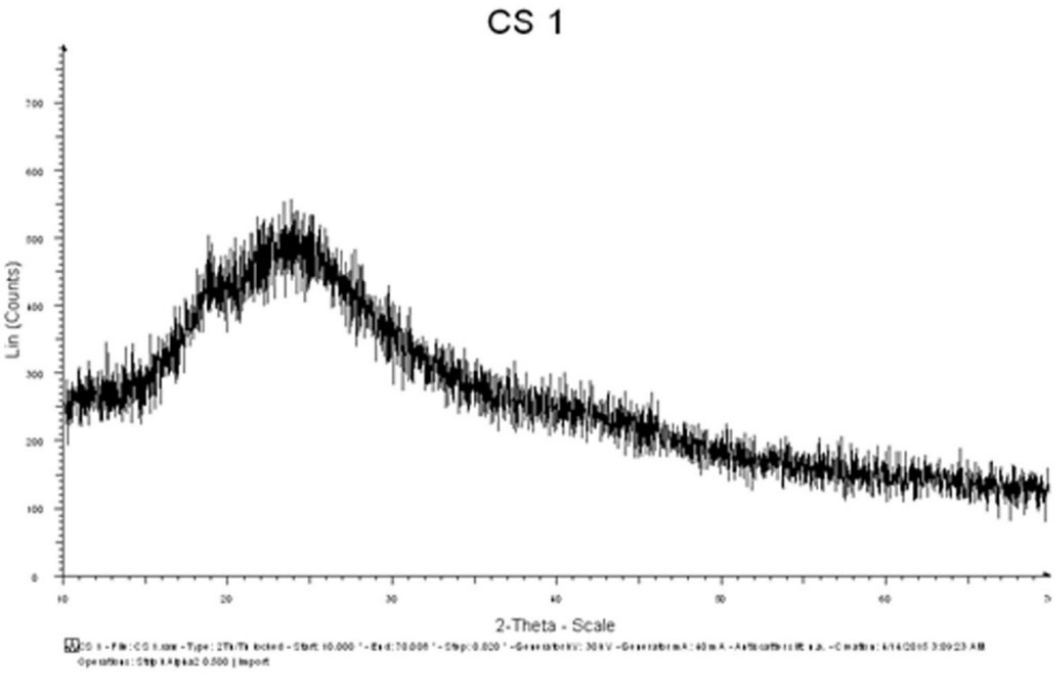

Fig. 6: X-ray powder diffraction patterns of chitosan nanoparticles.

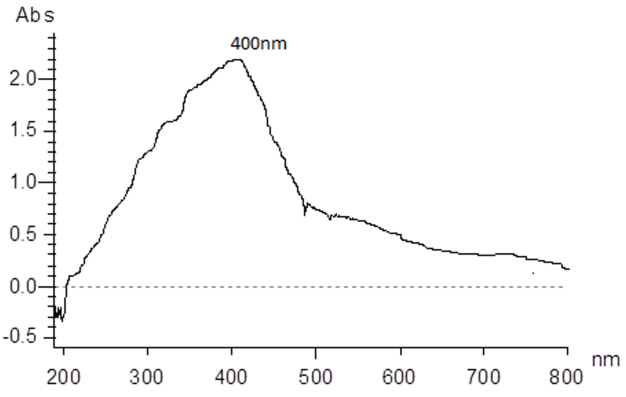

Fig. 7: UV-Visible spectrum of chitosan nanoparticles.

mg/L, 200 mg/L and 300 mg/L) of chitosan nanoparticles were added to 50 ppm blue dye and orange dye solution individually to determine the degradation efficiency of chitosan nanoparticles. After 60 and 180 mins interval maximum degradation were observed in the 300 mg/L nanoparticles concentration for both dyes compared to other two concentrations (Fig. 8 and Fig. 9). The percentage of degradation for blue dye was 67% approximately and nearly 56% for orange dye. Increase in the concentration of chitosan nanoparticles shows an increase in dye degradation for the first few minutes. The increase in degradation was probably due to an increase in availability of catalytic sites and adsorption sites. This is due to the fact that number of dye molecules adsorbed and photons absorbed increases with increase in photocatalyst concentration. The photodegradation of contaminant in water is usually due to the excitation of a semiconductor by UV light to produce free radicals, which aid the degradation of pollutant. The UV irradiation excited the electrons from valence band to conduction band, generating high-energy electron-hole pairs. The smaller size effect of the nanoparticles increased the energy band gap between the valence and conduction bands, increasing the redox potential and allowing UV light to be used more efficiently in photocatalysis (Chang & Juang 2004).

Pesticide degradation: The aqueous solutions of photo degraded pesticides were analysed by high performance liquid chromatography (HPLC). HPLC chromatogram confirms the formation and disappearance of intermediate compounds during photodegradation of profenofos and lambda cyhalothrin. Several small organic intermediates were formed. Retention time recorded for the major profenofos degraded compounds were 3.433, 6.933 and 7.333 min, whereas, for the lambda cyhalothrin retention times were 2.3333 and 3.233 min. The photodegradation of technical grade profenofos and lambda cyhalothrin was assessed using chitosan nanoparticles. HPLC were used to monitor the disappearance of profenofos and lambda cyhalothrin (Ahmed et al. 2011). The HPLC analysis showed that

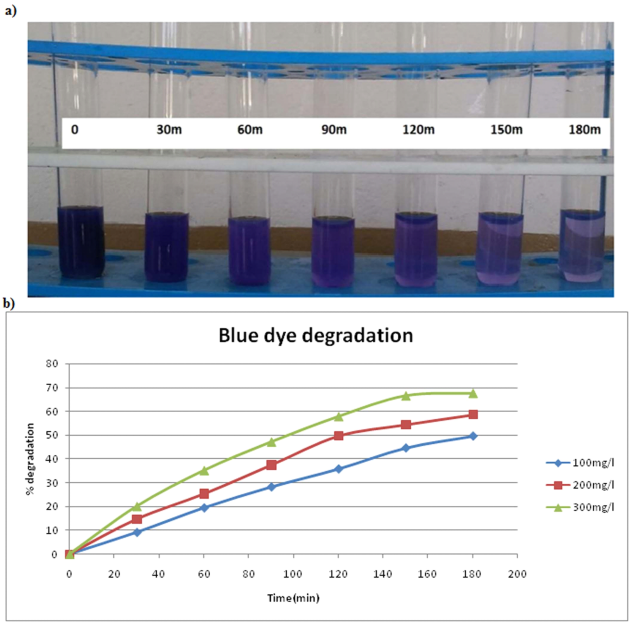

Fig. 8: (a) Degradation of blue dye at 0 min, 30 min, 60 min, 90 min, 120 min, 150 min and 180 min at 300mg/L of chitosan nanoparticles, (b) Percent degradation of blue dye at 100 mg/L, 200 mg/L and 300 mg/L.

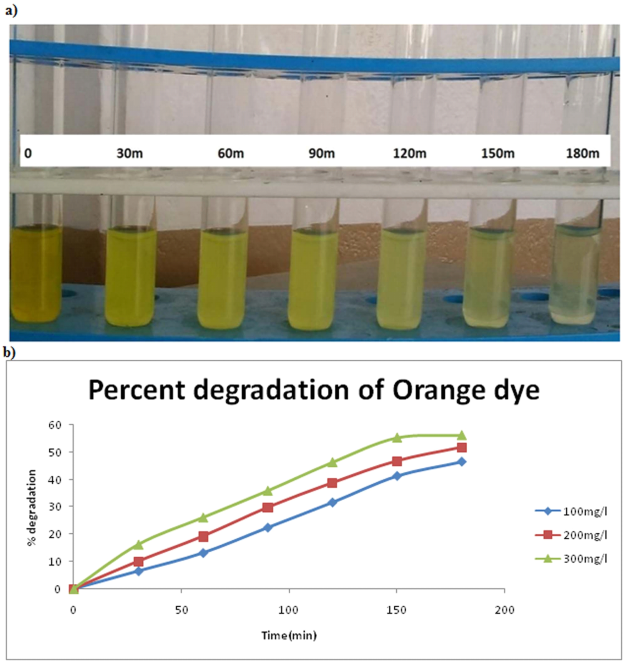

Fig. 9: (a) Degradation of orange dye at 0 min, 30 min, 60 min, 90 min, 120 min, 150 min and 180 min at 300mg/L of chitosan nanoparticles, (b) Percent degradation of orange dye at 100 mg/L, 200 mg/L and 300mg/L.

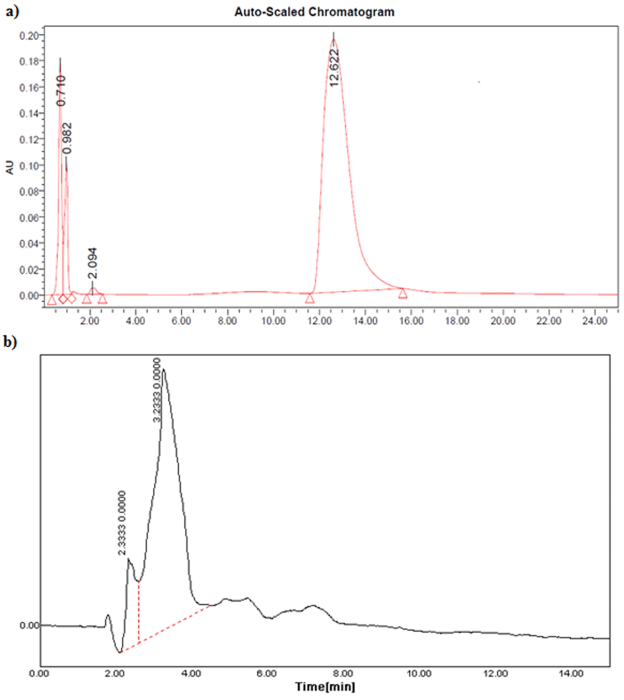

Fig. 10: (a) HPLC chromatogram of profenofos, (b) HPLC chromatogram after 6 days of incubation showing degradation of profenofos by chitosan nanoparticles.

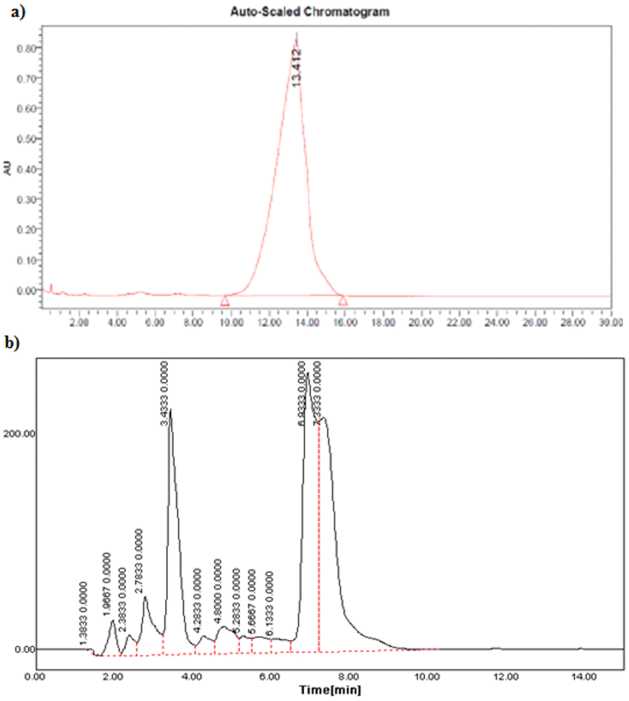

Fig. 11: (a) HPLC chromatogram of lambda cyhalothrin, (b) HPLC chromatogram after 6 days of incubation showing degradation of lambda cyhalothrin bychitosannano particles.

chitosan nanoparticles were able to efficiently degrade profenofos and lambda cyhalothrin. HPLC analyses results are shown in Figs. 10 and 11 and compared with the standard chromatogram of profenofos and lambda cyhalothrin. The HPLC analysis showed degradation of profenofos and lambda cyhalothrin by chitosan nanoparticle achieved after 6 days of incubation.

Adsorption kinetic studies: Kinetics is important for adsorption studies because it can predict the rate at which pollutant is removed from aqueous solutions and provides valuable data for understanding the mechanism of sorption reactions. In order to elucidate the adsorption process, two kinetic models including pseudo-first-order and pseudo-second order models were selected to fit the kinetic data. The linear form of the pseudo-first-order and pseudo-second-order kinetic models is given by:

$$\log (qe\text{-}qt) = \log qe - k1t \quad ...(1)$$

$$t/q_t = 1/k_2 q^2_e + t/q_c \quad ...(2)$$

Where, q_e and q_t are the adsorption capacities for adsorbent (mg/g) at equilibrium and at any time t, respectively; k1 is the rate constant of pseudo-first-order kinetic model. The values of k_1 and q_e can be determined from the slopes and intercepts of ln (q_e-q_t) vs. t plots; k_2 (g/mg min) is the rate constant of pseudo-second-order adsorption. The values of k_2 and q_e can be determined from the plots of t/q_t vs. t.

Effect of pH: The effect of pH on the dye removal was evaluated at different pH conditions ranging from 2 to 10. It shows the maximum adsorption at pH 4 for blue dye and pH 6 for lambda cyhalothrin. The maximum values of the adsorption capacity ratio between acidic and alkaline conditions reach 16.4 to 6.9 for blue dye on chitosan nanoparticle sorbent. The dye adsorption may also derive support from the ion exchange reaction. At lower pH more protons will be available to protonate amine groups of chitosan molecules to form groups -NH_3^+, thereby increasing electrostatic attraction between negatively charged dye anions and positively charged adsorption sites and causing an increase in dye adsorption. This explanation agrees with the data on pH effect. The effect of pH on blue dye and lambda cyhalothrin adsorption, was remarkable in the experimental conditions.

Effect of doses: Adsorbent dosage is an important factor which must be carefully optimized during wastewater treatment. The effect of dosage of chitosan nanoparticles on the removal of blue dye and lambda cyhalothrin was studied in various dosages.

The increase in blue dye removal efficiency with increasing adsorbent dosage is due to the increase of adsorption active sites on the adsorbent surface with the increase of adsorbent dosage. The point of saturation for chitosan nanoparticles was found at 300 mg/L for the removal of blue dye from aqueous solution. At saturation point, removal efficiency was found to be 48% for dye. There was no significant removal of dye observed above the saturation point because of the equilibrium between the dye molecules on the adsorbent and in the solution. Achievement of blue dye removal efficiency with a relatively low dosage of chitosan nanoparticles indicates the high affinity and suitability of chitosan nanoparticles for chitosan nanoparticles removal from water.

The effect of photocatalyst dosages on the adsorption of lambda cyhalothrin pesticide in aqueous solution was studied to obtain the optimum chitosan nanoparticles concentration. The experiments were carried out using different concentrations of chitosan nanoparticles ranging from 100mg/L to 600 mg/L. As the concentration of the photocatalyst increases from 100mg/L to 600mg/L, the adsorption efficiency of pesticide increases rapidly from lower to higher percentage. Then the efficiency decreases slightly when the amount of chitosan nanoparticles is above 600 mg/L. A further increase of the catalyst concentration beyond 600 mg/L may cause light scattering and screening effects. The excessive chitosan photocatalyst leads to opacity of the suspension, which prevents the catalyst farthest in solution from being illuminated.

Effect of time: The aqueous samples were taken at different time intervals and concentrations of dyes were comparably measured. The rapid removal was observed during the first 50 min and reached equilibrium within 90 min.

First, the kinetic data were fitted to the pseudo first-order kinetic model. Adsorption rate constants and their correlation coefficients were calculated from the linear plot. The validity of the model is checked by the correlation coefficient (R^2), and the calculated equilibrium adsorption capacities of both pseudo first-order and pseudo second-order. The applicability of the pseudo first-order kinetic model for chitosan nanoparticles on blue dye was examined by the linear plots of (t) vs log (q_e-q_t). Pseudo second-order was not fit well with the experimental data because of low (R^2). The adsorption correlation coefficient (R^2) of pseudo first-order was approximately close to unity, which fits the experimental data better than the pseudo second-order for the entire adsorption process (Fig. 12). Therefore, it can be concluded that pseudo-first-order equation is better in describing the adsorption kinetics of blue dye on chitosan nanoparticles and the rate of reaction appeared to be controlled by the chemical process.

The optimum amount of catalyst is found to be 600 mg/L for the adsorption study of the pesticide. The rela-

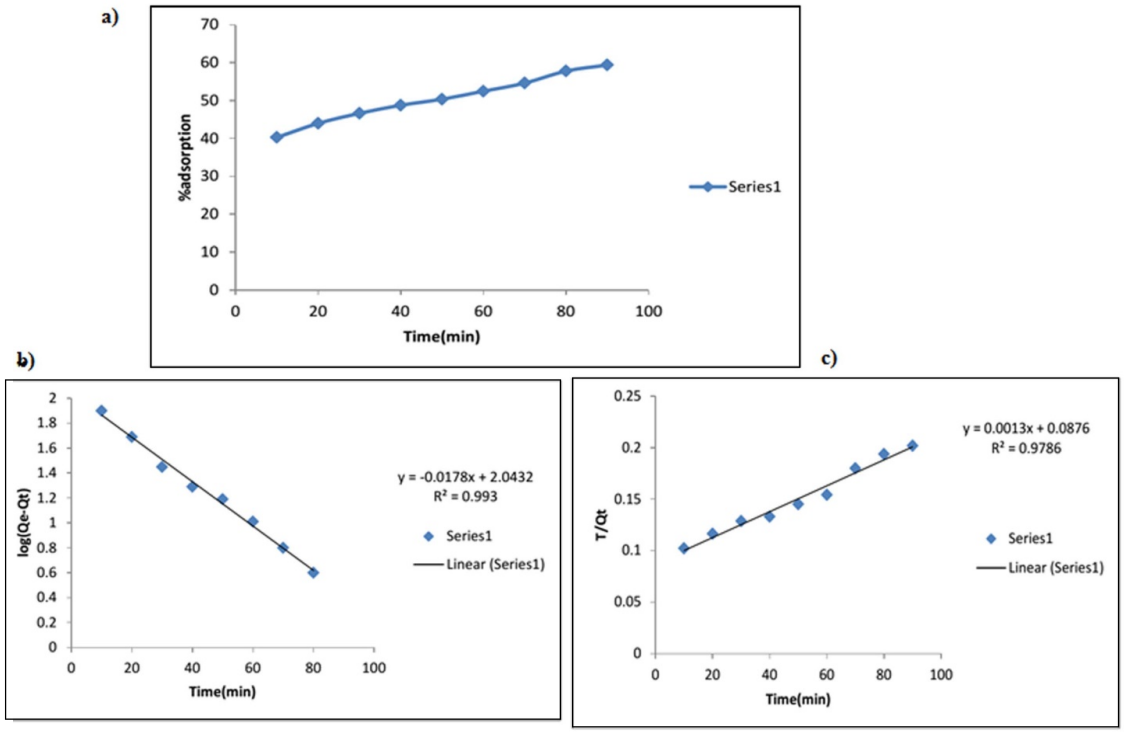

Fig. 12: (a) Percent adsorption of blue dye by chitosan nanoparticles over 100 min of time, (b) The pseudo first order kinetics of blue dye, (c) The pseudo second order kinetics of blue dye.

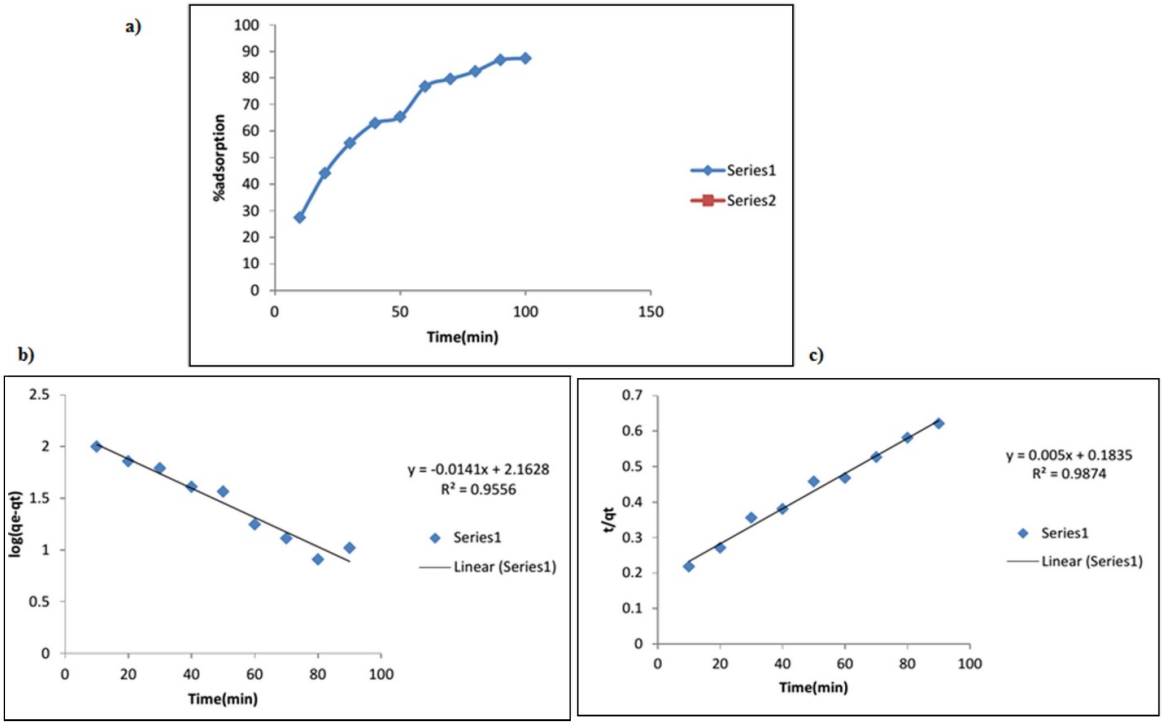

Fig. 13: (a) Percent adsorption of lambda cyhalothrin pesticide by chitosan nanoparticles over 100 min of time, (b) The pseudo first order kinetics of lambda cyhalothrin pesticide, (c) The pseudo second order kinetics of lambda cyhalothrin pesticide.

tionship between the adsorption efficiency of pesticide and the time was investigated and presented in Fig. 13. It can be seen that the adsorption efficiency of pesticide increases with the increase of the time showing that the adsorption efficiency of pesticide increases from 27.5% to 87.44% when the time increases from 10 to 100min. It can also be seen that with longer duration of about 70 min, only small enhancement of adsorption efficiency was observed. When the time was 90 and 100 min, the adsorption efficiency of pesticide was 86.83% and 87.44% respectively.

The kinetic data were modelled with the pseudo second-order kinetic equation, which shows the applicability of the pseudo second-order kinetic model for chitosan nanoparticles on lambda cyhalothrin which was examined by the linear plots of (t/qt) vs t. The adsorption correlation coefficient R^2 was approximately close to unity, which fits the experimental data better than the pseudo first-order for the entire adsorption process. Therefore, it can be concluded that pseudo-second-order equation is better in describing the adsorption kinetics of lambda cyhalothrin on chitosan nanoparticles.

The photocatalytic chitosan nanoparticles were used for environmental cleanup in degradation of the dyes and pesticides in the presence of the UV irradiation. The hazardous aqueous pollutants such as dye and pesticide were degraded successfully. The photocatalytic reactions occur on the surface of the pollutants after continuous UV irradiation. The percent reduction of dye and pesticide increases with the increase in duration of exposure but gives equilibrium constant after particular exposure time. At this point adsorption efficiency of photocatalyst stops and goes in equilibrium. The kinetic data were fitted with the pseudo first-order and pseudo second-order kinetic reaction, for the dye it was pseudo first-order and for pesticide it was pseudo second-order. This has prompted accelerated research activities worldwide on chitosan micro and nanoparticles as drug delivery vehicles.

CONCLUSION

The photocatalytic chitosan nanoparticles were used for environmental cleanup in degradation of the dyes and pesticides in the presence of the UV irradiation. The hazardous aqueous pollutants such as dye and pesticide were degraded successfully. The photocatalytic reactions occur on the surface of the pollutants after continuous UV irradiation. The percent reduction of dye and pesticide increases with the increase in duration of exposure but gives equilibrium constant after particular exposure time. At this point adsorption efficiency of photocatalyst stops and goes in equilibrium. The kinetic data were fitted with the pseudo first-order and pseudo second-order kinetic reaction, for the dye it was pseudo first-order and for pesticide it was pseudo second-order. This has prompted accelerated research activities worldwide on chitosan micro and nanoparticles as drug delivery vehicles.

REFERENCES

Ahmed, S., Rasul, M.G., Wayde, N.M., Brown, R. and Hashib, M.A. 2011. Advances in heterogeneous photocatalytic degradation of phenols and dyes in wastewater: A review. Water Air Soil Poll., 215(1): 3-29.

Amidi, M., Mastrobattista, E., Jiskoot, W. and Hennink, W.E. 2011. Chitosan-based delivery systems for protein therapeutics and antigens. Adv. Drug Deliv. Rev., 62: 59-82.

Berscht, P.C., Nies, B., Liebendorfer, A. and Kreuter, J. 1994. Incorporation of basic fibroblast growth factor into methylpyrrolidinone chitosan fleeces and determination of the in vitro release characteristics. Biomaterials, 15: 593-600.

Chang, M. and Juang, R. 2004. Adsorption of tannic acid, humic acid, and dyes from water using the composite of chitosan and activated clay. J Colloid Interface Sci., 278: 18-25.

Chauhan, R., Kumar, A. and Abraham, J. 2013. A biological approach to the synthesis of silver nanopartieles with *Streptomyces* sp JAR1 and its antimicrobial activity. Sci. Pharm., 81: 607-21.

Daneshvar, N., Aber, M.S. and Khataee, M.H. 2007. Photocatalytic degradation of the insecticide diazinon in the presence of prepared nanocrystalline ZnO powders under irradiation of UV-C light. Sep. Purif. Technol., 58(1): 91-98.

Dounighi, M.N., Eskandari, R., Avadi, MR., Zolfagharian, H., Mir Mohammad, S.A. and Rezayat, M. 2012. Preparation and in vitro characterization of chitosan nanoparticles containing Mesobuthuseupeus scorpion venom as an antigen delivery system. J. Venom Anim. Toxins., 18(1): 44-52.

Huang, H., Yuan, Q. and Yang, X. 2004. Preparation and characterization of metal-chitosan nanocomposites. Colloid Surface B., 39: 31-37.

Janes, A.K., Fresneau, M.P., Marazuela, A., Fabra, A. and Alonso, M.J. 2001. Chitosan nanoparticles as delivery systems for doxorubicin. J. Controlled Release, 73(2-3): 255-267.

Jayakumar, R., Anitha, V.V., Divya, R., Krishna, R., Sreeja, V. and Selvamurugan, N. et al. 2009. Synthesis, characterization, cytotoxicity and antibacterial studies of chitosan, O-carboxymethyl and N,O-carboxymethyl chitosan nanoparticles. Carbohydr. Polym., 78(4): 672-677.

Jiang, J., Oberdörster, G. and Biswas, P. 2009. Effect of molecular structure of chitosan on protein delivery. J. Nanopart. Res., 11(1): 77-89.

Katas, H., Raja, A.G., Leong, M. and Kai, L. 2013. Development of Chitosan nanoparticles as a stable drug delivery system for protein/siRNA. Int. J. Biomater., 20: 23-26.

Kavitha, T., Gopalan, A.I., Lee, K.P. and Park, S.Y. 2012. Glucose sensing, photocatalytic and antibacterial properties of graphene-ZnO nanoparticle hybrids. Carbon., 50: 2994-3000.

Knaul, J., Hudson, S.M. and Creber, K.A.M.J. 1999. Improved mechanical properties of chitosan fibres. Appl. Polym. Sci., 72: 1721-1731.

Lim, L.Y., Tang, E.S.K. and Huang, M. 2003. Ultrasonication of chitosan and chitosan nanoparticles, Int. J. Pharm., 265(1-2): 103-114.

Miretzky, P. and Cirelli, A.F. 2011. Fluoride removal from water by chitosan derivatives and composites: a review. J. Fluorine Chem., 132: 231-240.

Motwani, S.K., Chopra, S., Talegaonkar, S., Kohli, K., Ahmad, F.J. and Khar, R.K. 2008. Chitosan-sodium alginate nanoparticles as submicroscopic reservoirs for ocular delivery: Formulation, optimisation and in vitro characterization. Eur. J. Pharm. Biopharm., 68: 513-525.

Ngah, W.S.W., Teong, L.C. and Hanafiah, M.A.K.M. 2011. Adsorption of dyes and heavy metal ions by chitosan composites: a review. Carbohydr. Polym., 83: 1446-1456.

Patil, S., Sandberg, A., Heckert, E., Self, W. and Seal, S. 2007. Protein adsorption and cellular uptake of cerium oxide nanoparticles as a function of zeta potential. Biomaterials, 28(31): 4600-4607.

Qi, L., Xu, Z., Jiang, X., Hu, C. and Zou, X. 2004. Preparation and antibacterial activity of chitosan nanoparticles. Carbohydr. Res., 339(16): 2693-2700.

Singh, N., Chatterjee, A., Chakraborty, K., Chatterjee, S. and Abraham, J. 2016. Cytotoxic effect on MG-63 cell line and antimicrobial and antioxidant properties of silver nanoparticles synthesized with seed extracts of capsicum sp. Rec Nat Prod., 10: 147-157.

Tang, E.S.K., Huang, M. and Lim, L.Y. 2003. Ultrasonication of chitosan and chitosan nanoparticles. Int. J. Pharm., 265: 103-114.

Vimal, S., Taju, G., Nambi, K.S.N., Majeed, S.A. Sarath, B. and Ravi, V.M. et al. 2012. Synthesis and characterization of CS/TPP nanoparticles for oral delivery of gene in fish. Aquaculture, 358/359: 14-22.

Wang, H., Xie, C., Zhang, W., Cai, S., Yang, Z. and Gui, Y. 2007. Comparison of dye degradation efficiency using ZnO powders with various size scales. J. Hazard. Mater., 141(3): 645-652.

Yongmei, X. and Yumin, D. 2003. Effect of molecular structure of chitosan on protein delivery. Int. J. Pharm., 250: 215-226.